UC Irvine
UC Irvine Previously Published Works

Title

Short-term quantitative precipitation forecasting using an object-based approach

Permalink

https://escholarship.org/uc/item/5p35p8sr

Authors

Zahraei, Ali
Hsu, Kuo-lin
Sorooshian, Soroosh
et al.

Publication Date

2013-03-01

DOI

10.1016/j.jhydrol.2012.09.052

Short-term quantitative precipitation forecasting using an object-based approach

Ali Zahraei [a,*], Kuo-lin Hsu [a,1], Soroosh Sorooshian [a,1], Jonathan J. Gourley [b,2], Yang Hong [c,3], Ali Behrangi [d,4]

[a] Center for Hydrometeorology and Remote Sensing (CHRS), The Henry Samueli School of Engineering, Department of Civil and Environmental Engineering, University of California, Irvine, California, E/4130 Engineering Gateway, Irvine, CA 92697, United States
[b] NOAA/National Severe Storms Laboratory, Norman, Oklahoma, 120 David L. Boren Blvd., Rm. 4745, Norman, OK 73072, United States
[c] Department of Civil Engineering and Environmental Science, Atmospheric Radar Research Center, University of Oklahoma, Norman, Oklahoma, 120 David L. Boren Blvd., Rm. 4614, Norman, OK, United States
[d] NASA Jet Propulsion Laboratory, California Institute of Technology, Climate, Ocean, & Earth Science, 4800 Oak Grove Drive, Pasadena, CA, United States

SUMMARY

Short-term Quantitative Precipitation Forecasting (SQPF) is critical for flash-flood warning, navigation safety, and many other applications. The current study proposes a new object-based method, named PER-CAST (PERsiann-ForeCAST), to identify, track, and nowcast storms. PERCAST predicts the location and rate of rainfall up to 4 h using the most recent storm images to extract storm features, such as advection field and changes in storm intensity and size. PERCAST is coupled with a previously developed precipitation retrieval algorithm called PERSIANN-CCS (Precipitation Estimation from Remotely Sensed Information using Artificial Neural Networks-Cloud Classification System) to forecast rainfall rates. Four case studies have been presented to evaluate the performance of the models. While the first two case studies justify the model capabilities in nowcasting single storms, the third and fourth case studies evaluate the proposed model over the contiguous US during the summer of 2010. The results show that, by considering storm Growth and Decay (GD) trends for the prediction, the PERCAST-GD further improves the predictability of convection in terms of verification parameters such as Probability of Detection (POD) and False Alarm Ratio (FAR) up to 15–20%, compared to the comparison algorithms such as PERCAST.

1. Introduction

Short-term Quantitative Precipitation Forecasting (SQPF), or "nowcasting", is important for a number of hydrometeorological applications (Ganguly and Bras, 2003; Afshar et al., 2010). Both Numerical Weather Prediction (NWP) models and extrapolation-based techniques are widely used in SQPF. While these two methods are different in terms of their approaches, they play an effective and complementary role for SQPF (Golding, 1998; Ganguly and Bras, 2003; Wilson et al., 2004; Sokol, 2006; Liang et al., 2010).

Each of these methods has respective strengths and weaknesses (Wilson et al., 2004). Despite NWP models' applications in weather forecasting and SQPF, they are sensitive to the initial conditions, resolution, and assimilation algorithms (Golding, 1998). With high-frequency sampling of observations from new generations of sensor networks, the ability of NWP models to provide short-term predictions is substantially improved over the US (Benjamin et al., 2004, 2009). Although there have been significant improvements in NWP models and their broad range of applications, they may still have some limitations. For example, NWP models are associated with significant computational cost, which poses limitations in terms of spatial domain, resolution, frequency, and the number of ensemble members. Extrapolation-based or "data-driven-based" algorithms, however, are capable of extracting information from the ever-increasing volume of remotely sensed data and are reported to be capable of producing reliable forecasts with respect to NWP models, especially within a few hours of the analysis time (Dixon and Wiener, 1993; Johnson et al., 1998; Germann and Zawadzki, 2002, 2004; Mueller et al., 2003; Ganguly and Bras, 2003; Chiang et al., 2006; Vila et al., 2008; Zahraei et al., 2010a, 2010b; Sokol and Pesice, 2012).

Several extrapolation-based nowcasting algorithms have been developed for hydrological applications. The Storm Cell Identification and Tracking (SCIT) algorithm and the Thunderstorm Identification, Tracking, Analysis, and Nowcasting (TITAN) algorithm are two examples (Johnson et al., 1998; Dixon and Wiener, 1993). Integration of some of these algorithms into the National Weather

---

* Corresponding author. Present address: NOAA-CREST, United States.
  E-mail addresses: azahraei@ccny.cuny.edu (A. Zahraei), kuolinh@uci.edu (K.-l. Hsu), soroosh@uci.edu (S. Sorooshian), Jj.Gourley@noaa.gov (J.J. Gourley), yanghong@ou.edu (Y. Hong), ali.behrangi@jpl.nasa.gov (A. Behrangi).
  [1] Tel.: +1 949 824 9350; fax: +1 949 824 8831.
  [2] Tel.: +1 405 325 6472; fax: +1 405 325 1774.
  [3] Tel.: +1 405 325 3644.
  [4] Tel.: +1 818 393 8657.

Service (NWS) Warning Decision Support System (WDSS) has been reported (Lakshmanan et al., 2009).

Pixel- and object-based are two categories of data-driven SQPF algorithms. There have been several proposed pixel-based quantitative precipitation estimation and forecasting algorithms (Grecu and Krajewski, 2000; Mecklenburg et al., 2000; Germann and Zawadzki, 2002; Montanari et al., 2006; Vant-Hull et al., 2008; Berenguer et al., 2011; Zahraei et al., 2011a, 2012). These algorithms study atmospheric phenomena from an Eulerian, pixel-based perspective. Object-based quantitative precipitation estimation and forecasting algorithms, which are the main focus of this paper, consider storm events as individual objects (Dixon and Wiener, 1993; Hong et al., 2004; Vila et al., 2008).

An object-based algorithm generally includes three steps: (1) storm identification, (2) storm tracking, and (3) storm projection. The identification and matching/tracking of each storm object at the current time (t) with the corresponding storm in the previous time step(s) (e.g., $t − 1$, $t − 2$, etc.) is a major challenge for nowcasting and storm life-cycle studies. Storms are dynamic in terms of intensity, texture, and geometrical characteristics. They may also split or merge with other storms, which makes the application of tracking algorithms very challenging (Machado and Laurent, 2004). Several object-based storm-tracking methods have been proposed (Lakshmanan et al., 2009), including: (1) storm-matching technique based on centroid positions (Johnson et al., 1998); (2) storm-cell matching based upon the proposed indices of overlapping pixels (Morel et al., 1997); and (3) a modified approach where storm tracking and association has been solved as an optimization problem (Dixon and Wiener, 1993).

These tracking techniques have not been without limitations. For example, the centers of mass methods are not robust in processing complex-shaped objects effectively. The overlapping technique performs well for large storm systems (e.g., Mesoscale Convective Systems, MCSs), in which storm objects are large enough to allow sufficient overlap in consecutive time steps (Lakshmanan et al., 2009; Vila et al., 2008). However, for small-scale thunderstorms, they cannot be tracked effectively using overlapping techniques. Other proposed techniques also assume that storm objects are long-lived and large enough to be associated with previous time steps (Lakshmanan et al., 2009). Although object-based algorithms are effective for SQPF, they need further improvements. As an example of newly developed object-based nowcasting algorithms, the Forecast and Tracking the evolution of Cloud Cluster (ForTraCC) has been proposed to identify, track, and forecast MCSs (Vila et al., 2008). This nowcasting tool was applied to evaluate MCS evolution up to 120 min with a 30-min interval over southern America.

In this study, a new object-based SQPF algorithm capable of tracking and forecasting storms is developed and described. The proposed algorithm, named PERCAST (PERsiann-ForeCAST), can identify and track storms from GOES-IR (infrared) cloud-top long-wave Brightness Temperature (BT) data. The term "storm" presents all atmospheric phenomena with cloud BT less than a specific threshold (e.g., 240 K) and area larger than 256 km². The performance of PERCAST is verified against both radar and satellite data and compared with two comparison SQPF models: (1) PERsistence (PER), and (2) WDSS-II (Warning Decision Support System-Integrated Information). The PER assumes that the future rainfall field is equal to the last available scan. The WDSS-II, developed by the National Severe Storm Laboratory (NSSL) and the University of Oklahoma, is frequently used for the identification, tracking, and nowcasting of thunderstorms (Lakshmanan et al., 2009).

The methodology of the proposed nowcasting model is presented next, followed by applied data sets, case studies, results and verification, conclusions, and appendices.

2. Methodology

The PERCAST algorithm predicts rainfall rates in the next 4 h (240 min) using infrared satellite imagery (GOES channel 10.8 μm) with time intervals of about 30 min between two consecutive satellite observations. Literature shows that a time interval of 15–30 min between two observations can be appropriately used to track storm features (Morel and Senesi, 2002; Vila et al., 2008).

There are three major steps in PERCAST, as presented in Fig. 1: (1) storm identification, (2) storm tracking, and (3) storm projection. The steps are described in detail in the following sections.

2.1. Storm identification (segmentation)

For the object-based nowcasting algorithms, effective storm segmentation is the first step. Mature convective storms can penetrate to high altitudes and, therefore, they show overshooting tops and are well associated with colder cloud BT. While BT less than 245 K can satisfactorily identify MCSs, usually the temperature between 228 K and 235 K has been proposed for the summer season, which is based on the assumption that deep convection penetrates in the upper troposphere (Machado et al., 1998; Vila et al., 2008). Vila et al. (2008) proposed a 235 K threshold for MCS nowcasting studies. The proposed PERCAST algorithm would process both mesoscale (e.g., MCS) and small-scale storm events that could not be processed through a single thresholding screening (Lakshmanan et al., 2009). It has been documented that, for cloud and precipitation studies, especially at weather scale, a single BT threshold is not robust due to seasonal, regional, and climatological variability (Adler et al., 1994; Machado et al., 1998). Even multiple threshold techniques have been reported to be problematic for severe storms (Lakshmanan et al., 2009). Therefore, a more advanced segmentation algorithm, called the watershed transform algorithm, has been applied (Roerdink and Meijster, 2001; Lakshmanan et al., 2009; Hong et al., 2004, 2005) (Appendix A).

2.2. Storm tracking and association

By defining contiguous pixels that are segmented in each storm object, matching a storm at the current time (t) with the storm's corresponding location in the previous time step(s) (e.g., $t − 1$, $t − 2$, etc.) is a major concern for each nowcasting model. In addition, the PERCAST algorithm needs to track both large- and small-scale events, which create more complexity.

The PERCAST model tracks storms at pixel scale, which connects pixels in two consecutive time steps through the cloud-image advection vectors (Bellerby, 2006). Further, the overlapping pixels within each segmented storm-coverage area from time t to $t − 1$ are estimated. A backward-forward tracking process connects pixels in storm objects from time t to $t − 1$. The contribution/tracking of a storm object from $t − 1$ to another storm at time t can be calculated based on a proposed contribution function, as discussed below.

First, assume that there are two consecutive image objects at time $t − 1$ and t, which correspond to the same storm/cloud, where:

- O is an object at time $t − 1$, and $A(O)$ is the area of O,
- $O′$ is an object at time t, and $A(O′)$ is the area of $O′$.

The contribution function between O and $O′$ (Eq. (1)) is calculated based on the number of pixels (area) being connected from the object $O′$ at time t to O at time $t − 1$ (Morel and Senesi, 2002).
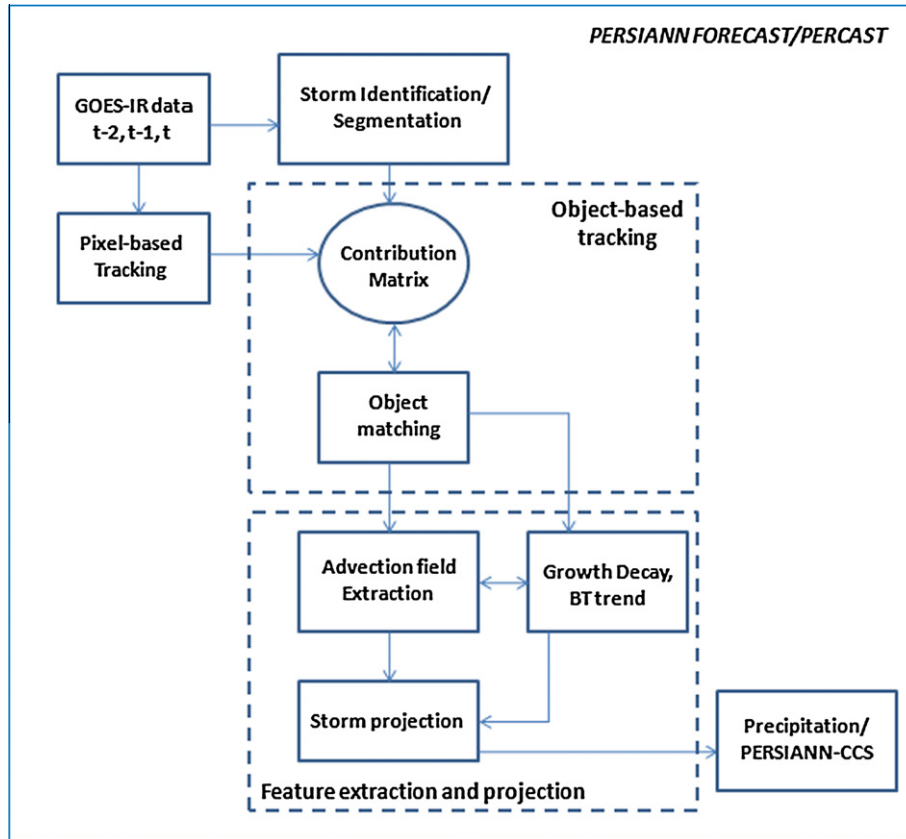
Fig. 1. The flowchart of the PERCAST algorithm for precipitation short-term forecasting using satellite information.

$$\text{Contribution function } \{F_{O',O}\} = \frac{A(O\prime) \text{ originally from } A(O) = (O \cap O')}{A(O')} \tag{1}$$

$$0 \leqslant \sum_{i=1}^{\text{No. of objects } t-1} F_{O',i} \leqslant 1 \tag{2}$$

The contribution function (Eq. (1)) indicates the probability of object O' contributed from the object O in the previous time step $t-1$. Using the pixel-based clouds tracking, PERCAST is able to find the corresponding location of each pixel in the previous time steps (Bellerby, 2006; Zahraei et al., 2011b, 2012). Tracking pixels between times $t-1$ and t extracts the advection of pixels from $t-1$ to t. Thus, instead of the simple assumption of direct overlapping of clouds (e.g., Vila et al., 2008), the common area along the advection trajectory of pixels covered by two objects O and O' in two successive time steps can be calculated, which is listed as the numerator in Eq. (1). Because each object at time t is usually linked to one or a few storm object(s) at time $t-1$, the summation of the contribution function for each object at time t will be between 0 and 1 (Eq. (2)). The value "1" is the case of objects at time $t-1$ being fully contributed to the specific object at time t, while a value "0" indicates that there was no contribution of objects at time $t-1$ to t that could be a newly generated storm at time t. The object-based overlapping area of the shared pixels of the storm using the advection trajectory in two consecutive time steps is calculated for all objects from time $t-1$ (e.g., O) to t (e.g., O'). The proposed tracking algorithm is able to directly associate the evolution of mesoscale and local convective thunderstorms (Appendix B).

It has been documented that there may be five different situations among the objects, including (1) continuity, (2) spontaneous generation, (3) dissipation, (4) split, (5) merger, and (6) combinatorial (Mathon and Laurent, 2001; Vila et al., 2008). The backward-and-forward tracking process using the contribution function makes it possible to consider all situations.

Fig. 2 displays the matching of image objects at two consecutive time steps from $t-1$ to t. At time $t-1$, there are five objects, including A, B, C, D, and E, whereas at time t, there are six storm objects, including A', B', C', D', E', and F'.

2.2.1. Continuity

The common area between two objects from time steps $t-1$ and t implies that these two objects are from the same storm that has evolved from $t-1$ to time t, i.e., Fig. 2a shows that objects D and D' are matched. However, it is much more complicated when an object at time $t-1$ is connected with two or more objects at time t. A minimum separation threshold is needed to identify the correct associations for storm objects evolving in time (Morel and Senesi, 2002) (separation threshold – Appendix B).

2.2.2. Generation

Using a backward–forward tracking process, if there is no contribution of a storm object from time t to $t-1$, the storm object at time t can be a storm which has just initiated. For objects E' and F' at time t, if the contribution function is equal to 0, it means that none of the storm objects from a previous time step are associated with them (E' and F') (Fig. 2b). Those objects are considered as new storms.

2.2.3. Dissipation

Similar to the generation situation, if there is no contribution of storm objects from time steps $t-1$ to t, the storm can be a dissipated one. Fig. 2c shows that object E at time $t-1$ has disappeared.
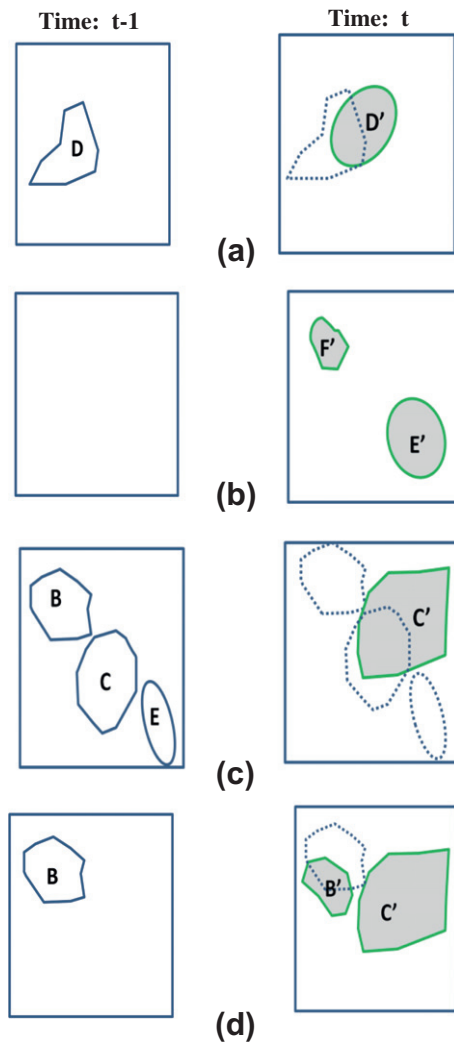
Fig. 2. Schematic representation of two consecutive identified storm objects at time $t-1$ and t. (a) Continuity, (b) generation, (c) dissipation and merger, and (d) split. There are five and six objects at time $t-1$ and t, respectively. The matching process will match the corresponding storms using the proposed object-based tracking algorithm.

2.2.4. Split

When a specific object at time $t-1$ is associated with two or more objects at time t, the result can be the split case. In the case of splitting an object into two or more objects, the largest connected object at time t will be assigned the identification number of the contributed objects from time $t-1$. From Fig. 2d, object B could be split into B' and C'. Objects B and B' are matched together. The contribution of object B in C' is ignored because it is not significant (less than the separation threshold ~ 0.25, Appendix B).

2.2.5. Merger

If two or more objects at time $t-1$ are connected to an object at time t, a merger has occurred. For example, Fig. 2c shows that objects C, B, and E at time $t-1$ might contribute to generating object C' at time t. The backward-and-forward tracking process shows that only objects C and E have contributed to object C', while the portion of object B that has contributed to C' is not significant (Appendix B).

2.2.6. Combinatorial

The most complicated cases are those in which two or more of the aforementioned situations occur simultaneously, i.e., the case

in which both merging and splitting occur for one specific storm object. For example, Fig. 2c and d shows that object B at time $t-1$ could split to B' and partly merge to object C' at time t, while the object-matching process shows that object B only significantly contributes to object B', and contribution to object C' is not significant (Appendix B).

2.3. Storm projection

After the storm segmentation/identification and tracking process, a trajectory for each specific storm from time t to $t-1$, $t-2$, etc. is assigned. Two different scenarios are used to project (extrapolate) the storm. The first scenario, named PERCAST, uses two consecutive time steps, $t-1$ and t, to extract the storm-advection field (velocity) and uses a fixed velocity to project the storm forward in time (Fig. 3a). The second scenario, called PERCAST-GD, further considers Growth and Decay (GD) along with trends in BT and area of the storm (Fig. 3b). The PERCAST-GD algorithm uses three consecutive time steps, t, $t-1$, and $t-2$, to identify and track storm objects. Given the fact that each storm is now tracked through previous time steps, the projection module can extrapolate the storm. The proposed algorithm projects storms through the following four steps: (1) storm velocity/advection estimation, (2) feature extractions such as geometric (area), radiance (BT minimum, BT average), and gradients of features, (3) storm-position prediction, and (4) storm intensity and size prediction. The first two steps extract storm features and variations (gradients of features from $t-2$ to $t-1$ and t) in addition to each storm advection velocity which will be used by PERCAST-GD for projection. Once the storm is projected, the rainfall algorithm will convert cloud BT to the rate of rainfall. Calculation of each of the four modules will be discussed below.

2.3.1. Storm-velocity estimation

Considering each storm trajectory, the velocity $V(C')$ of a cell C' at time t can be defined using the center of mass location (Morel and Senesi, 2002):

If C' is a newly generated object at time t, then $V(C')$ is the velocity of the nearest cell at time t. If the center of mass of the nearest object is farther than 500 km from the center of mass of C', the $V(C')$ will be considered as 0. Otherwise:

$$V(C') = \frac{1}{2}\frac{CC'}{\Delta t} \qquad (3)$$

where CC' is the distance between the center of mass of C at time $t-1$ and C' at time t.

Literatures propose that, instead of calculating the storm-velocity estimation based on the instantaneous speed, it should be calculated based on an average of the object trajectories in the previous time steps (e.g., three time steps, $t-2$ to $t-1$ and $t-1$ to t) (Morel and Senesi, 2002). The PERCAST-GD uses the average velocity of object C moving from time step $t-2$ to $t-1$ (object C') as velocity $V(C)$, and object C' at $t-1$ moving to the object C'' at time t as velocity $V(C')$. Eq. (4) calculates the velocity of a given object at time t. Two parameters, a and b, show that the velocity is a linear combination of each storm object trajectory $C \rightarrow C' \rightarrow C''$.

$$\text{Velocity} = aV(C) + bV(C') \qquad (4)$$

The current case studies have revealed that an assumption of $a = b = 0.5$ is reasonable.

2.3.2. Storm features extraction

Storm features (e.g., cloud BT/intensity) may change as storms move and evolve. Each convective storm may have three life stages, including initiation, maturity, and dissipation. Newly generated convective storms typically have a strong updraft, and the
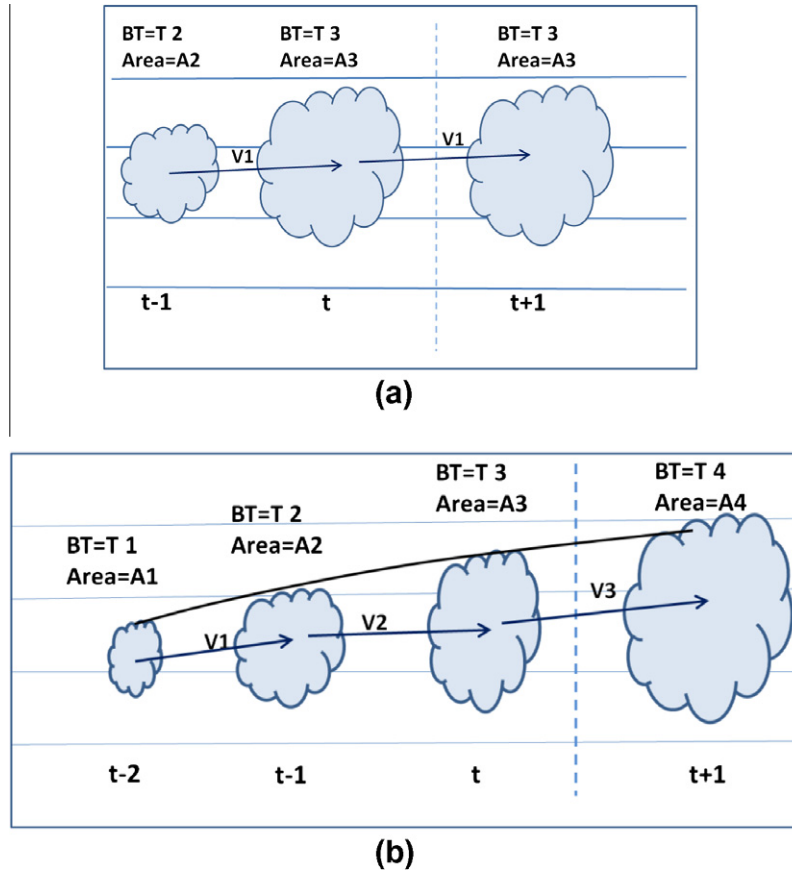
(a)

(b)

Fig. 3. (a) PERCAST, two consecutive time steps $t - 1$, and t. The storm grows upward, and it becomes larger and colder, $A_2 < A_3$, and $T_2 > T_3$, PERCAST does not consider trends; (b) PERCAST-GD, three consecutive time steps $t - 2$, $t - 1$, and i. The storm grows upward, and it becomes larger and colder, $A_1 < A_2 < A_3$, and $T > T_2 > T_3$. V is the 2-D advection vector for the storm, V_3 = average($V_1 + V_2$).

BTs at cloud-top become colder and larger in size. Thus, there are important dynamic trends in BT and size. PERCAST-GD considers the aforementioned feature changes and trends. Each of these feature changes might be partially important for an operational algorithm intended to provide global short-term precipitation forecasts (Appendix C).

2.3.3. Storm-position prediction

The estimated advection field (velocity) will be applied to project each storm object position. The PERCAST and PERCAST-GD algorithms apply the last 30 min and the average of the last 1-h advection, respectively. The model extrapolates each storm for the next 4 h using the estimated advection field. However, it should be noted that, similar to other algorithms (e.g., Vila et al., 2008), this nowcasting model has shown its merit in the very short-term forecasting up to ∼2 h.

2.3.4. Storm intensity and size extrapolation

As time passes, storm position, as well as its BT and geometric features at cloud-top, typically change. The PERCAST-GD algorithm extracts storm BT and area changes from previous time steps. When a convective storm grows and becomes colder in terms of BT, the average BT of the object at time $t - 1$ is usually lower than the corresponding average BT at time $t - 2$. Thus, there are usually cooling (negative) trends in BT. Furthermore, the minimum temperature of the growing convective storm is usually lower at time $t - 1$ than its corresponding minimum temperature at time $t - 2$. However, there are some exceptions; while the average BT is decreasing, the minimum BT may not be necessarily changing.

Hence, the PERCAST-GD algorithm applies a linear combination of two trends ($\Delta BT_{\min}$ and ΔBT_{mean}), as follows:

$$\Delta BT = c\Delta BT_{\text{mean}} + d\Delta BT_{\min} \qquad (5)$$

where ΔBT_{mean} and $\Delta BT_{\min}$ are the average and minimum BT trends, respectively (Appendix C). c and d are weighting parameters. Different case studies have shown that equal coefficients ($c = d = 0.5$) are reasonable.

When convection is growing, the storm usually becomes larger in size and colder in BT. Therefore, the extrapolation algorithm should be able to adjust storm size as well, meaning that each storm has a growth-decay trend in size. The algorithm measures the average of trends to project the storm size (Appendix C) (Fig. 3b). This trend will be applied at the first extrapolated time step ($t + 1$), and then will be reduced linearly to about zero from $t + 2$ to $t + 8$ to avoid unreasonable values (Scofield et al., 2004). In addition, each object should not grow larger than 100% at each time step (∼30 min). The accumulated growing factor is also prevented from reaching a maximum threshold (e.g., 250–300%) in the next 4 h (Scofield et al., 2004). Similarly, a lower bound is used to control the minimum size that the storm is allowed to shrink.

In summary, the projection procedure includes two different parts, including storm advection, size, and BT prediction. The growth-decay factor can be particularly useful for providing more accurate predictions of changing convective storms.

2.3.5. Rainfall forecast

Using the aforementioned procedure, the PERCAST algorithm will be able to nowcast storms. This paper applies PERSIANN-
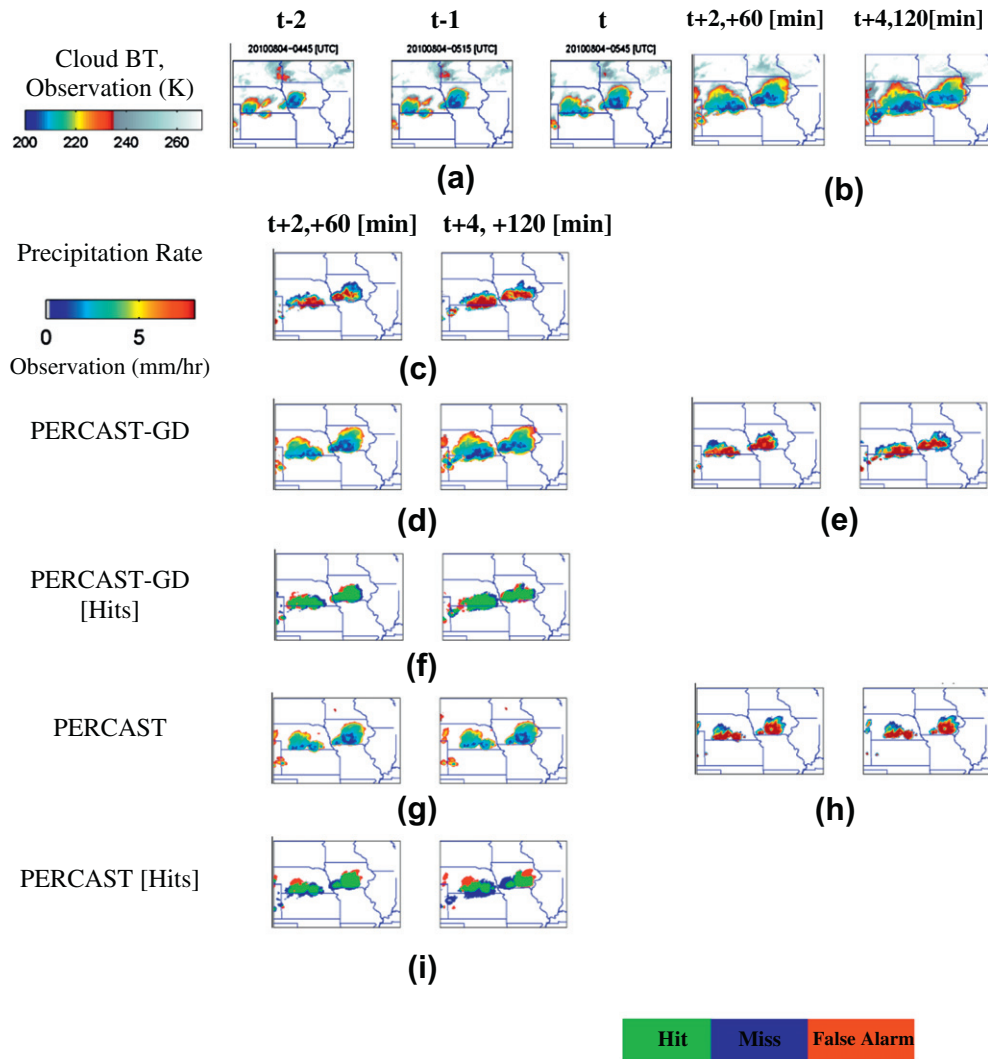
Fig. 4. Case study on 4 August 2010, the most recent cloud BT and observation, as well as the PERCAST-GD and PERCAST algorithms, cloud BT, and rate of rainfall. Hits from predicted vs. CCS and radar Q2 observation. (a) Three consecutive cloud-BT imageries (rainfall >1 mm/h). (b) Cloud-BT observation for +60 ($t + 2$) and +120 ($t + 4$) [min]. (c) Precipitation rate, CCS observation ($t + 2$, $t + 4$). (d) Predicted PERCAST-GD (cloud BT) for +60 ($t + 2$) and +120 ($t + 4$) [min] lead time. (e) PERCAST-GD corresponding predicted rate of rainfall for (d). (f) Hits from PERCAST-GD (e) vs. PERSIANN-CCS observation which is (c). (g) Predicted PERCAST (cloud BT) for +60 and +120 [min] lead time. (h) PERCAST corresponding predicted rate of rainfall for (g). (i) Hits from PERCAST (h) vs. observation (c), less hits more missing compared to (f).

Table 1
PERCAST and PERCAST-GD algorithms, POD and FAR, for the event shown in Fig. 4, including +60 and +120 [min] lead time.

Nowcasting	POD	FAR	CSI	Nowcasting	POD	FAR	CSI
PERCAST lead time = 60 min	0.57	0.37	0.42	PERCAST lead time = 120 min	0.41	0.51	0.24
PERCAST-GD lead time = 60 min	0.70	0.31	0.53	PERCAST-GD lead time = 120 min	0.63	0.42	0.38

CCS to estimate the rainfall rates of the projected/forecasted storms (Hong et al., 2004). The PERSIANN-CCS algorithm includes a hybrid-segmentation module, a feature-extraction module, and the ANN module. The first two modules have already been briefly explained. The ANN module is a Self-Organizing Nonlinear Output (SONO) network to classify cloud objects into a similarity-based family of clusters using a Self-Organizing Feature Map (SOFM) (Hsu et al., 1999; Hong et al., 2005; Behrangi et al., 2009). Then, multi-parameter nonlinear functions are calibrated to identify the relationship between the classified cloud objects and their associated precipitation using the Probability Matching Method and the Multi-Start Downhill Simplex optimization technique.

3. Data

The PERCAST-GD model is evaluated using GOES-IR data over a rectangular region between 80°W to 115°W and 32°N to 45°N. The primary forcing data are the full-resolution IR data available from the Climate Prediction Center (CPC) that covers the continental Unites States (CONUS) and adjacent oceans (Janowiak et al., 2001). This data set provides a 0.04° × 0.04° spatial resolution, a 30-min composite of available GOES-IR imagery that is originally blended from GOES-E and GOES-W satellites. Over the study area, summertime precipitation is dominated by convective storms associated with MCS systems that traverse the Great Plains typically during nighttime hours (Ashley et al., 2003).
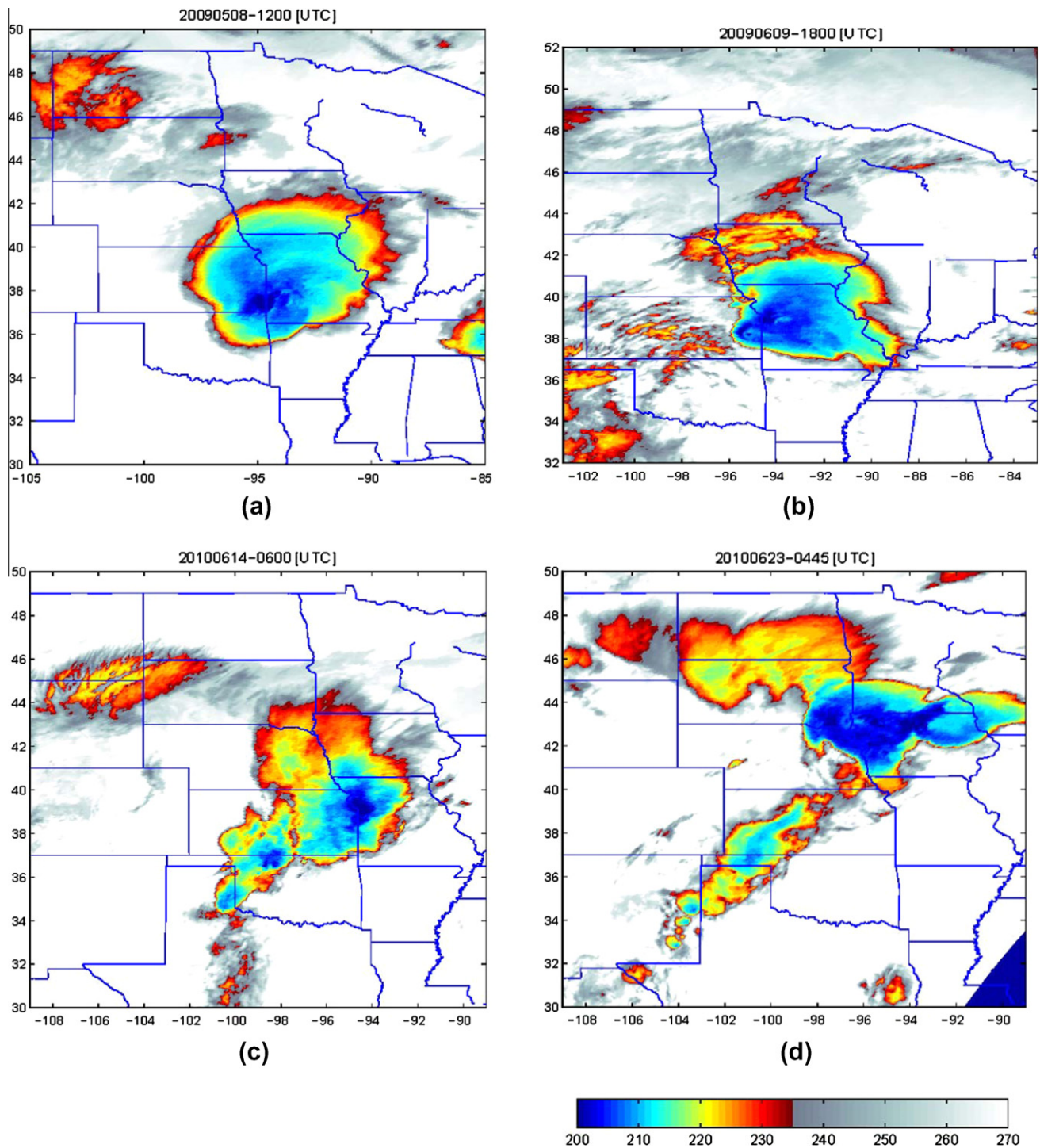
Fig. 5. Four selected severe storms, GOES-IR observations: (a) Event 1: 20090508-1200 [UTC], (b) Event 2: 20090609-1800 [UTC], (c) Event 3: 20100614-0600 [UTC], and (4) Event 4: 20100623-0450 [UTC] (Unit: Brightness Temperature = K).

Rainfall estimates from the NEXRAD-based National Mosaic and QPE system (Q2; Zhang et al., 2011) are used for comparison and evaluation of the proposed algorithms. Q2 is a state-of-the-art rainfall estimation system which has significantly mitigated the effects of non-weather contaminants, such as insects, anomalous propagation, and ground clutter and mosaics rainfall estimates into $0.01° \times 0.01°$ grids every 5 min (Lakshmanan et al., 2007; Vasiloff et al., 2007). For the purposes of this study, the Q2 data have been resampled to the IR satellite resolution.

4. Results

Both PERCASST and PERCAST-GD nowcasting scenarios have been verified vs. both satellite-based observed rainfall (PERSI-ANN-CCS) and ground-based radar rainfall observation. As it was mentioned the proposed model estimate rainfall using projected storms and PERSIANN-CCS. Thus, there are two sources of uncertainty regarding the storm projection and rain-

Table 2
Information for four storms/events during 2009–2010, including time, length, and states damaged by the storm. The last three columns show if the storms had severe winds, flash flooding, and/or tornados. *Source:* National Climate Data Center; ncdc.noaa.gov.

Event	Time [mm/dd/yy]	Length [h]	States	Severe wind	Flash flood	Tornado
1	05/08/09	18	KS, MO, KY, VA	Yes	Yes	Yes
2	06/[09–10]/09	18	KS, MO	Yes	Yes	Yes
3	06/[13–14]/10	24	OK, KS	Yes	Yes	Yes
4	06/[22–23]/10	21	NE, SD, IA, WI	Yes	Yes	Yes

Table 3
POD, FAR, and CSI, for four selected storms using PERCAST-GD, PERCAST, WDSS-II, and PER models vs. PERSIANN-CCS observation. Lead time +30 min.

Model	+30 (min)				
	Index	Event 1	Event 2	Event 3	Event 4
PERCAST-GD	POD	0.65	0.68	0.59	0.54
	FAR	0.39	0.37	0.46	0.49
	CSI	0.40	0.42	0.33	0.32
PERCAST	POD	0.59	0.62	0.5	0.5
	FAR	0.44	0.44	0.49	0.53
	CSI	0.34	0.36	0.27	0.25
WDSS	POD	0.56	0.58	0.48	0.46
	FAR	0.45	0.46	0.54	0.55
	CSI	0.31	0.32	0.21	0.19
PER	POD	0.48	0.51	0.46	0.41
	FAR	0.49	0.53	0.56	0.58
	CSI	0.22	0.21	0.19	0.16

Table 4
POD, FAR, and CSI, for four selected storms using PERCAST-GD, PERCAST, WDSS-II, and PER models vs. PERSIANN-CCS observation. Lead time +60 min.

Model	+60 (min)				
	Index	Event 1	Event 2	Event 3	Event 4
PERCAST-GD	POD	0.58	0.6	0.54	0.44
	FAR	0.44	0.48	0.43	0.52
	CSI	0.32	0.32	0.27	0.2
PERCAST	POD	0.49	0.52	0.44	0.39
	FAR	0.52	0.6	0.56	0.57
	CSI	0.25	0.22	0.18	0.16
WDSS	POD	0.43	0.47	0.41	0.38
	FAR	0.54	0.59	0.59	0.62
	CSI	0.2	0.18	0.16	0.14
PER	POD	0.34	0.34	0.36	0.3
	FAR	0.6	0.66	0.63	0.68
	CSI	0.11	0.09	0.12	0.08

fall estimation. To discriminate different errors, the PERSIANN-CCS observations are also compared with the radar-observed rainfall (Q2).

Five performance measures are used for verification of PER-CAST-GD including: (1) Correlation Coefficient (CC), (2) Probability of Detection (POD), (3) False-Alarm Ratio (FAR), and (4) Critical Success Index (CSI) and (5) Odds ratio. They measure the agreement between forecast (F) and observation (O) (Legates and McCabe, 1999; Grecu and Krajewski, 2000; Hogan et al., 2009). Grecu and Krajewski (2000) stated that POD, FAR, and CSI are better metrics for pattern matching. POD shows the ability of the forecasting algorithm in prediction of rainy/non-rainy pixels, based upon predefined thresholds. FAR indicates instances in which the storm is predicted while there is no storm. CSI shows how well the predicted storm corresponds to the observed storm. Hogan et al. (2009) also indicated that POD and FAR have limitations in characterizing forecasting skill. Stephenson (2000) represents the odds ratio as a complementary verification measure.

5. Models evaluation

The efficacy of both SQPF scenarios, PERCAST and PERCAST-GD, is evaluated with four case studies. The first case study evaluates a single convective storm event. The second case study shows the application of the proposed model to nowcast four severe storm events. The third evaluation is based on average monthly forecasting skill. Estimations from PERCAST and PERCAST-GD algorithms with forecasting lead times up to 240 min using the entire month of May 2010 are evaluated over the entire study area. The fourth evaluation covers five successive months May, June, July, August, and September 2010. The comparison and evaluation of the proposed algorithm is conducted over the entire study region for storms greater than 256 km^2.

5.1. Case Study I: Evaluation for a single event

Fig. 4 displays the application of both PERCAST and PERCAST-GD algorithms for an event on 5:45 UTC 4 August 2010, over the
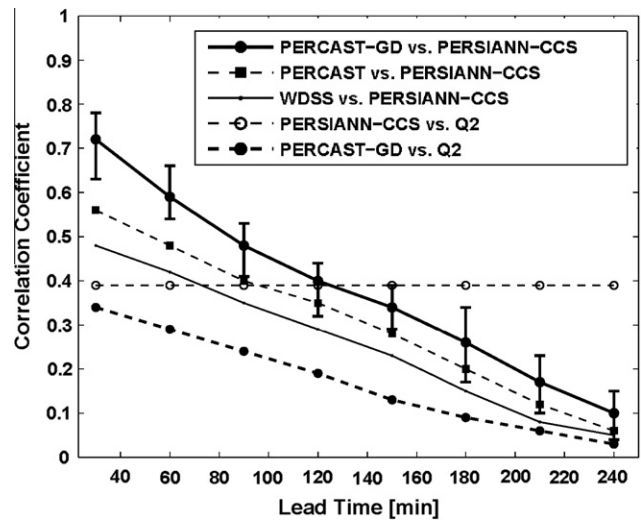

Fig. 6. The Correlation Coefficient (CC) vs. lead time [min] on average for May 2010. The PERCAST + Growth–Decay (GD) algorithm, the PERCAST, the WCN/WDSS-II, and PERsistency (PER) have been plotted. The PERCAST-GD prediction vs. the Q2 radar data is also plotted. The PERSIANN-CCS vs. the Q2 radar shows the application of the rain-conversion algorithm compared to the radar observation. Bars show the minimum, maximum, and average values of the correlation coefficients for May 2010, for PERCAST-GD. The first forecasting time (lead time) is $t + 1 = +30$ (min).

Midwest US. Fig. 4a shows three consecutive time steps of GOES-IR cloud imagery (BT) in which two separate convective activities start growing at the same time. Fig. 4b displays the next two time steps ($t + 2$ and $t + 4$), including +60 min and +120 min cloud BT observations, respectively. Fig. 4c illustrates the corresponding precipitation rate estimated from PERSIANN-CCS for the storms depicted in Fig. 4b. Fig. 4d gives the projected storm using PERCAST-GD, and Fig. 4e provides the PERCAST-GD corresponding predicted rainfall. Fig. 4f shows the hit, missing, and false alarms with the PERCAST-GD forecast compared with PERSIANN-CCS observations. Fig. 4g displays the projected storm using the PERCAST algorithm, and Fig. 4h gives the PERCAST corresponding
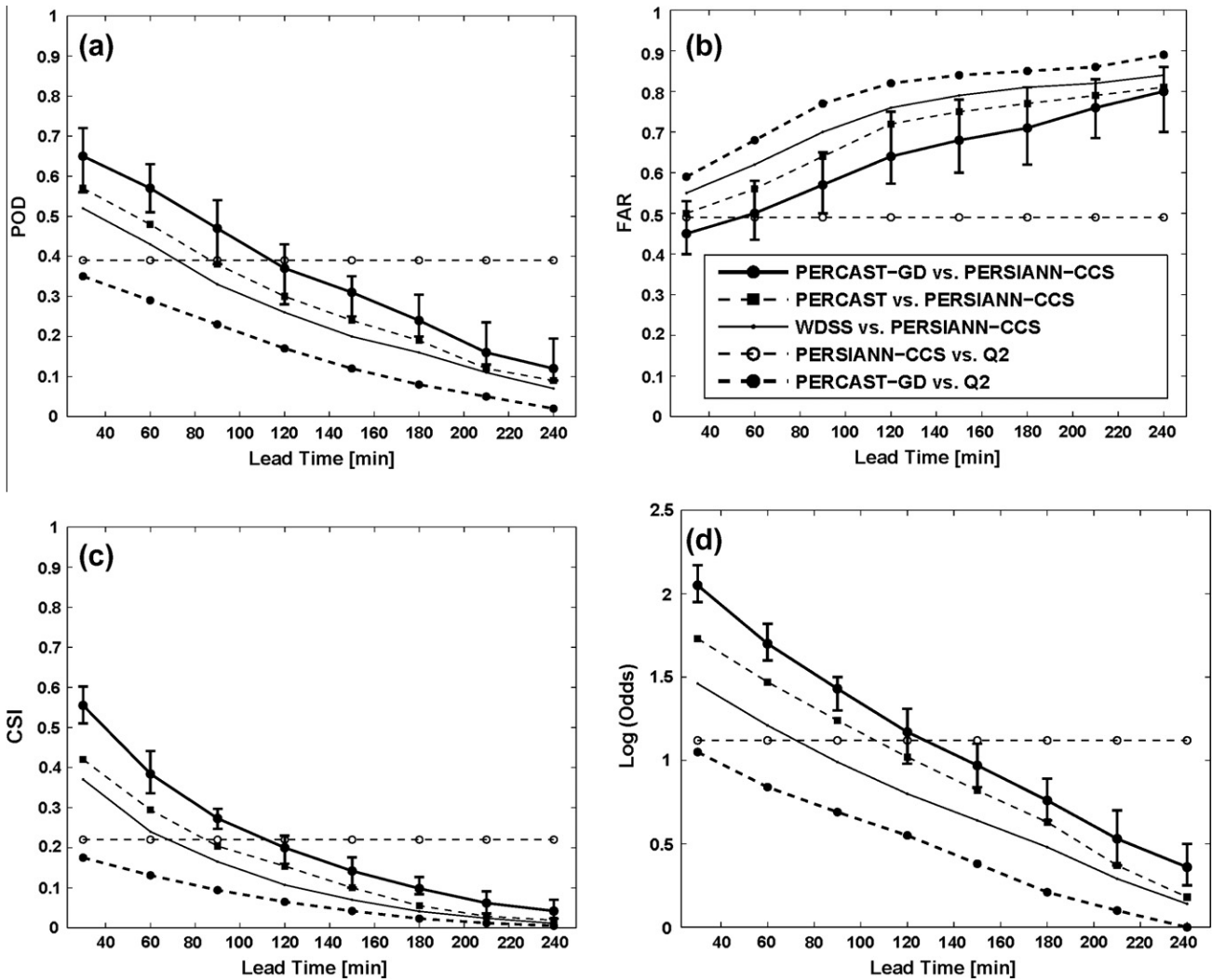
Fig. 7. (a) The Probability of Detection (POD) vs. lead time [min] for May 2010, PERCAST, PERCAST-GD, WDSS-II, and PER. The PERCAST-GD algorithm is compared with real-time radar observations. The precipitation estimation algorithm (PERSIANN-CCS) is compared with radar (Q2) data. (b) The False-Alarm Ratio (FAR) vs. lead time [min] for May 2010, PERCAST, PERCAST-GD, WDSS-II, and PER. The PERCAST-GD vs. real-time radar observation Q2, and PERSIANN-CCS vs. (Q2) data. (c) The Critical Success Index (CSI) vs. lead time [min] for May 2010, PERCAST, PERCAST-GD, WDSS-II, and PER. PERCAST-GD vs. real-time radar observation Q2, and PERSIANN-CCS vs. radar (Q2) data. (d) Logarithm of Odds ratio vs. lead time [min] for May 2010, PERCAST, PERCAST-GD, WDSS-II, and PER. PERCAST-GD vs. real-time radar observation Q2, and PERSIANN-CCS vs. radar (Q2) data. Bars show the minimum, maximum, and average values of the POD, FAR, CSI, and Log (Odds) for PERCAST-GD. The first forecasting time (lead time) is $t + 1 = +30$ (min).

predicted rainfall. Fig. 4i shows the hit, missing, and false alarms with the PERCAST forecast compared with PERSIANN-CCS observations. A comparison of Fig. 4e and h shows that the PERCAST algorithm predicts storm advection based on the storm movement from time steps t and $t − 1$ reasonably well, whereas the PERCAST-GD predicts both storm advection and convection growth more accurately, as it is designed to do.

Considering Fig. 4a–i and Table 1, the PERCAST-GD could more accurately forecast advection and evolution of the growing convective activities; for example, comparing Fig. 4f and i shows that the POD of PERCAST-GD and PERCAST in lead time of 120 min are 63% and 41%, respectively. Therefore, the PERCAST-GD may be considered a relatively more reliable precipitation forecasting tool, particularly for convective dominant events/seasons.

5.2. Case Study II: Very short term severe storms nowcasting

The second case study involves the evaluation of the proposed models in nowcasting specific severe storms. Four relatively severe storm events over the contiguous United States (CONUS) area are

selected (Fig. 5). They have produced severe winds, flash floods, or tornadoes (Table 2). All storms have caused either human fatalities or significant property damage. The selected storms are fast-evolving with complicated structures, and they all produced intense rainfall. In addition, the third storm is a unique, relatively stationary storm producing more than 250 mm of rainfall in less than 6 h over Oklahoma.

Four SQPF models have been used, including PER, WDSS-II, PERCAST, and PERCAST-GD. WDSS-II works with a modified definition of clustering using size criteria (Lakshmanan et al., 2009). Also, it applies the tracking algorithm proposed by Morel and Senesi (2002) to match storms.

Given the fact that this is an event-based case study, a dynamic window traveling with each storm has been applied. Throughout the storm life cycle, this window moves with the storm and isolates it from neighboring events to evaluate the performance of the proposed algorithms for that specific severe storm. Each forecast is updated every 30 min (Δt) with new satellite observation, using few consecutive time steps (t = current time) and ($t − \Delta t$, $t − 2\Delta t$ = previous time steps).
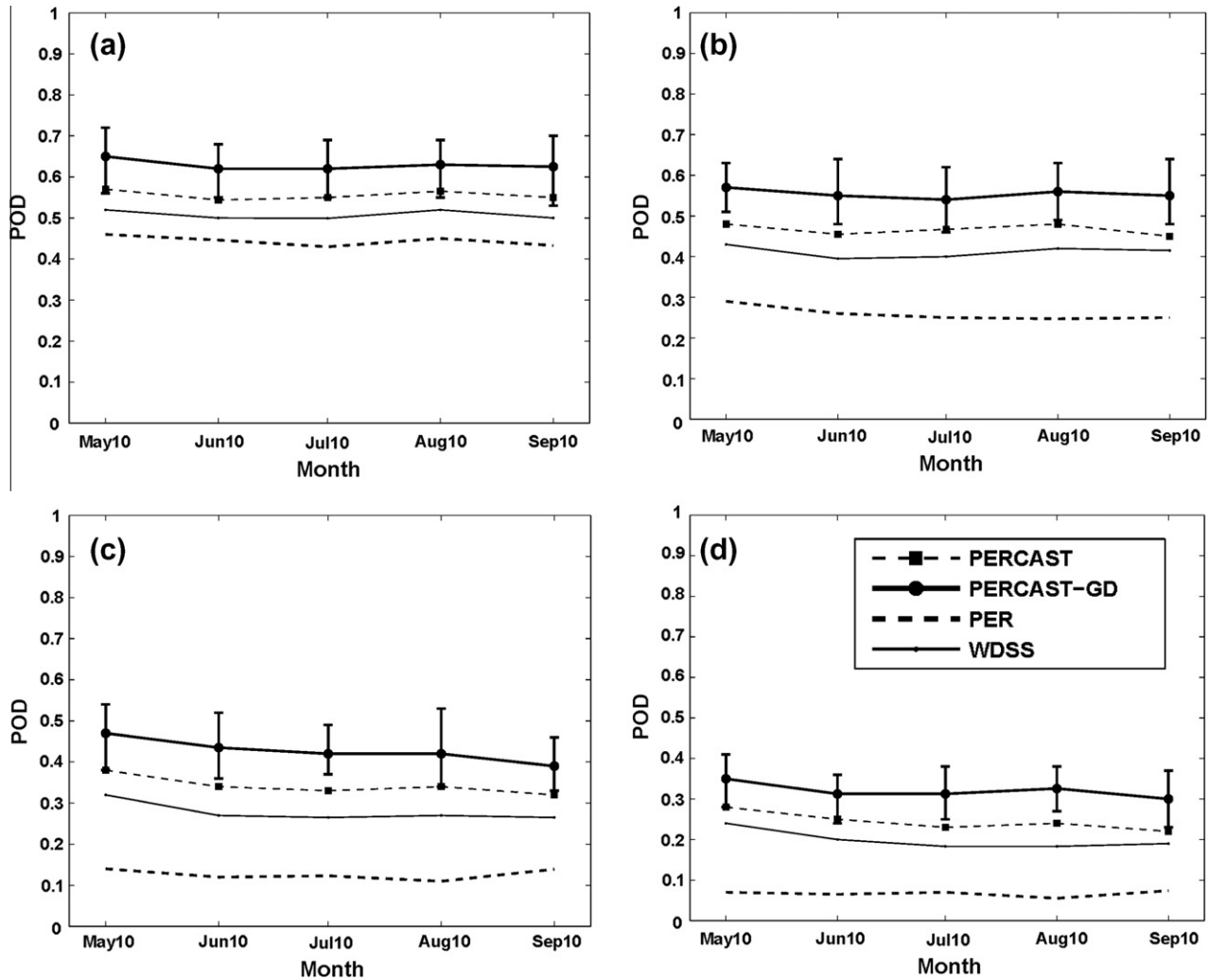
Fig. 8. Probability of Detection (POD) vs. time [month] including May, June, July, August, and September 2010 for rainfall >1 [mm/h], using PERSIANN-CCS as observation. (a) +30 [min] prediction. (b) +60 [min] prediction. (c) +90 [min] prediction. (d) +120 [min] prediction. Bars show the minimum, maximum, and average values of the POD for PERCAST-GD.

In Tables 3 and 4, performance of PERCAST-GD, PERCAST, WDSS-II and PER models are compared. According to Tables 3 and 4, the PERCAST-GD shows improved performance in very short-term forecasting (30 and 60 min lead time), and PERCAST and WDSS-II perform in a relatively similar manner. Considering the GD and BT trends and robust advection fields of the convective storms, PERCAST-GD is slightly superior to the comparisons models. Assuming there is a newly generated and growing storm, the applied growth trend could enhance POD of the growing storm. Also, the decay trend minimizes FAR ratio when a convective storm dissipates.

On the other hand, PER which is a control model has shown the worst performance amongst the other models, except for the third storm which is relatively stationary.

5.3. Case Study III: Evaluation of May 2010

The third evaluation focuses on forecasting skill vs. lead time for the entire month of May 2010, over the previously mentioned study domain. WDSS-II, PERCAST, and PERCAST-GD, have been applied with every 30 min update.

Figs. 6 and 7 illustrate the application of the three models against the PERSIANN-CCS rainfall observation, PERCAST-GD vs. Q2 and PERSIANN-CCS vs. Q2 observation which are averaged over the entire domain for May 2010. The verification measures have been used to show the skill of the SQPF algorithms in the next 4 h (from lead time = +30 min, and every 30 min). It is observed that, in terms of CC, POD, FAR, CSI, and odds ratio statistics, the PERCAST-GD algorithm is relatively more accurate, as compared to both PERCAST and WDSS-II.

In the first couple of minutes of lead time (e.g., +30, +60, etc.), all algorithms perform well. The forecasting ability of extrapolation-based SQPF algorithms decreases with increasing lead time. In Fig. 6, considering an acceptable Correlation Coefficient (CC) threshold of ~35–40%, which is the CC of PERSIANN-CCS observation vs. radar Q2 observation (a flat line averaged for the entire spatial–temporal study domain), shows that the PERCAST and PERCAST-GD algorithms are capable of providing effective forecasts for the next ~90 and ~120 min, respectively.

Fig. 7 indicates the superiority of using the PERCAST-GD algorithm vs. comparison algorithms using POD, FAR, CSI, and the logarithm of the odds ratio for May 2010. Overall, the proposed PERCAST-GD has provided acceptable forecasts in the first 2 h; after that, all models begin to lose their merit and merge toward each other. In addition, the extended lead time (up to 4 h) reveals that extrapolation-based SQPF models may not have any efficacy after 4 h.
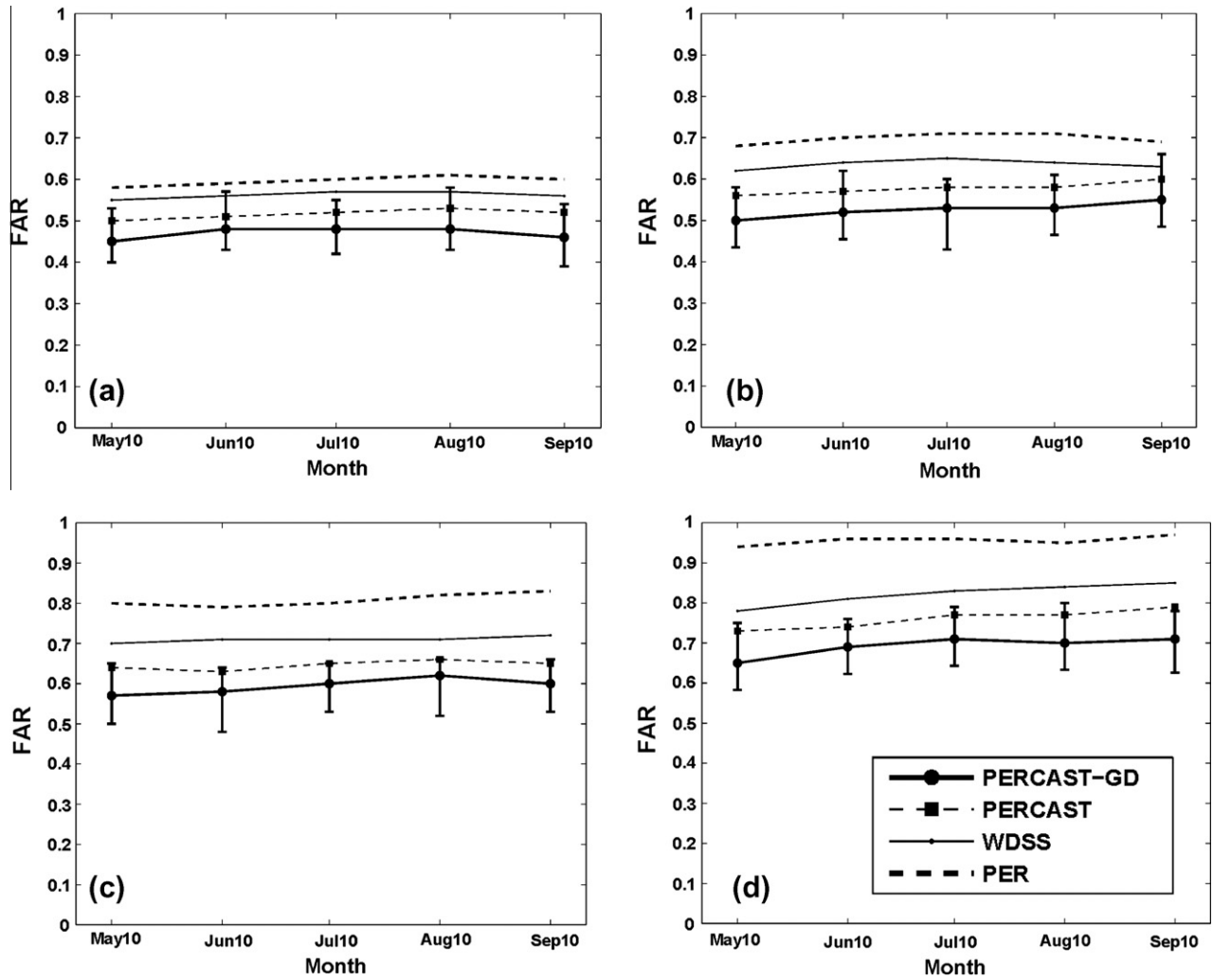
Fig. 9. False-Alarm Ratio (FAR) vs. time [month] including May, June, July, August, and September 2010 for rainfall >1 [mm/h], using PERSIANN-CCS as observation. (a) +30 [min] prediction. (b) +60 [min] prediction. (c) +90 [min] prediction. (d) +120 [min] prediction. Bars show the minimum, maximum, and average values of the FAR for PERCAST-GD.

As previously mentioned, there are two sources of errors: (1) projection error, and (2) precipitation estimation error of the projected storm. The projection error can be investigated by comparing the forecasts with precipitation estimates from PERSIANN-CCS (e.g., PERCAST-GD vs. PERIANN-CCS; Figs. 6 and 7). The precipitation estimation (PERSIANN-CCS) errors due to the conversion of observed brightness temperatures to precipitation rates is identified by comparing PERSIANN-CCS with Q2 estimates, as flat lines shown in Figs. 6 and 7 (PERSIANN-CCS vs. Q2), assuming Q2 estimates as "truth". Therefore, comparing PERCAST-GD vs. PERSIANN-CCS, and Q2 observations, the former only present the error in projection algorithm, while the latter presents the total SQPF error. The gap between the PERCAST-GD vs. Q2 observation and PERSIANN-CCS vs. Q2 observation (flat line) is assigned to the forecasting algorithm. This difference is initially minor and gradually increases in longer lead time (e.g., after 90–120 min). If the projection algorithm did not have any error, PERCAST-GD vs. Q2 would merge to the flat line.

Figs. 6 and 7 also reveal that the main priority of using the proposed PERCAST-GD algorithm might be its ability to identify and track local evolving convective storms which are likely to become very severe thunderstorms. These storms might produce significant amounts of rainfall, while other comparison algorithms have been unable to accurately identify and track them (e.g., WDSS-II).

Adequate tracking of storms is generally considered a prerequisite for accurate SQPF.

In addition, according to Germann et al. (2006), there are a few other important factors affecting forecasting skill, such as the scale dependency. The fact that the selected case studies contain short lifetime and fast-evolving small-scale storms, might be a reason for the relative drop in the forecasting skill after a few minutes of forecasting (e.g.,+30 min lead time).

5.4. Case Study IV: Monthly evaluation (May, June, July, and August 2010)

The previous example showed the forecasting skills of the proposed models for a single month (May 2010) vs. lead time, in which there was a decreasing trend in forecasting skill vs. lead time up to 240 min. In those instances where the proposed PERCAST-GD model performed relatively robust in the first 120 min, models arguably lose their capabilities beyond 120 min. Therefore, this case study evaluates the efficacy of PERCAST-GD over 5 months, for lead time up to 2 h. The verification statistics include POD and FAR at forecast lead times of +30, +60, +90, and +120 min.

As shown in Figs. 8 and 9, the +30-min prediction is more reliable than +60 min and so on. The ability of PERCAST and PERCAST-GD to perform better is due to their ability to more accurately
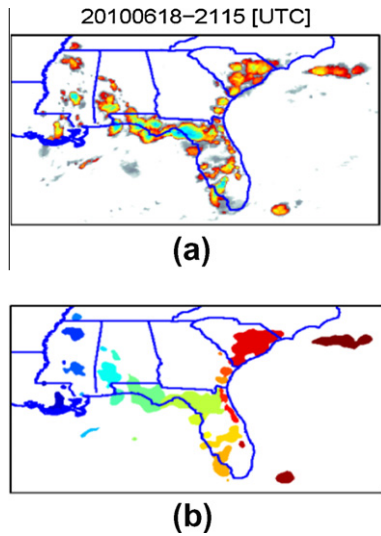
Fig. A1. (a) GOES-IR observation, 2010618-21:15 [UTC]. (b) Segmented image using watershed transform algorithm.

Fig. A2. The contribution matrix, objects at time $t - 1$ (A, B, etc.) and t (A', B', etc.).

identify and track a broader range of storms. Additionally, the consistent performance of PERCAST-GD is superior to that of PERCAST and other comparison algorithms. For example, Fig. 8 shows that PERCAST-GD outperforms others and is followed by PERCAST for all prediction lead times. Relatively speaking, the PERCAST-GD algorithm improves the predictability of storms (particularly convective storms) about 15–20% compared to PERCAST. The GD, as well as the intensity-change components, significantly enhance the capability of the PERCAST-GD algorithm.

Therefore, considering the broad range of global satellite information, the proposed algorithm may be used as an SQPF tool. The PERCAST-GD algorithm is relatively efficient for operation over the contiguous US and can be extended for precipitation forecasting worldwide.

6. Conclusions

Two object-based algorithms, called PERCAST and PERCAST-GD, suitable for detecting important storm features (e.g., size and intensity trends) were applied and verified. The basic PERCAST algorithm uses two consecutive time steps to track and project the storm, while the PERCAST-GD algorithm considers three previous consecutive time steps, along with the cloud-brightness temperature and GD trends. Forecast precipitation fields are estimated based on IR features at cloud-top. Verification results using standard statistical tests demonstrate the superior performance of PERCAST-GD for short-term forecasts over comparison algorithms.

PERCAST and PERCAST-GD were applied for precipitation forecasting, and their performances were compared to the WDSS-II and PER using single storm events and 5 months of data during the warm season (May–September) in 2010. Although the WDSS-II algorithm could usually capture storm advection and significantly outperform the PER model, the verification results based on the standard statistical tests show that both PERCAST and

$$A \rightarrow A'+F'(split) \rightarrow A'$$
$$B \rightarrow (split)B'+C' \rightarrow B'$$
$$C + B + E(merger) \rightarrow C'$$
$$D \rightarrow D'$$
$$E \rightarrow Dissipation$$
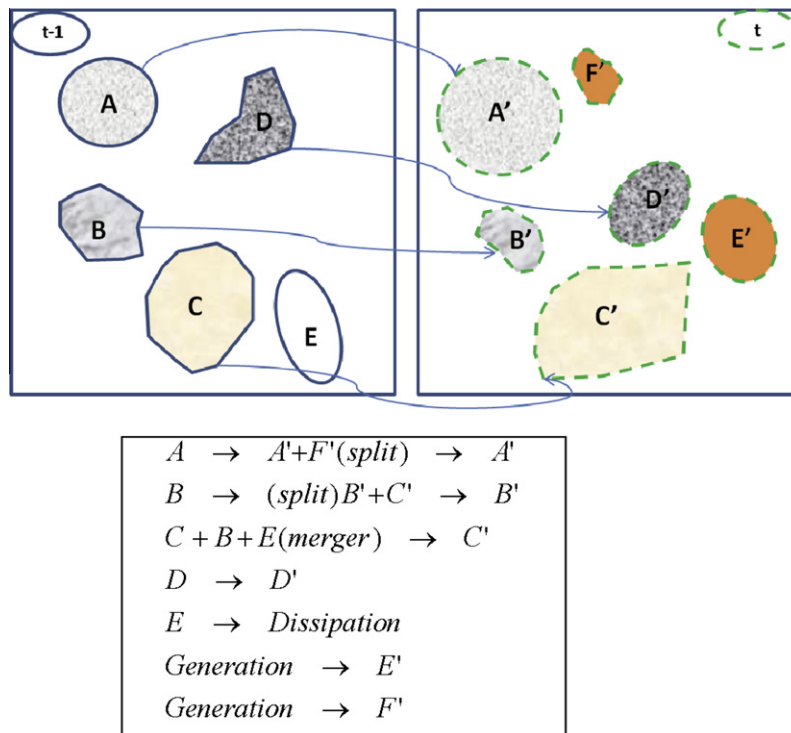$$Generation \rightarrow E'$$
$$Generation \rightarrow F'$$

Fig. A3. According to the contribution matrix (Fig. A2), matching corresponding objects. (a) The top-left box belongs to objects at time $t - 1$, and the box on the right belongs to objects at time t. Objects are associated from $t - 1$ to t. (b) Storm matching using contribution matrix.

PERCAST-GD perform relatively better. The PERCAST-GD algorithm has the best overall performance.

Using POD, FAR, CSI, the odds ratio, and CC reveals that PERCAST-GD improves the predictability of convective storms about 15–20% compared to PERCAST. Considering the CC between the PERSIANN-CCS observation and radar observation that is about 35–40% as the threshold, the PERCAST algorithm forecasts well in the first 90 min. Using the same threshold, the PERCAST-GD improves predictability by about 30–45 min up to ∼120 min.

While this is the first part of the current research that is more focused on the methodology, and while initial results are encouraging, more complex and advanced forecasting scenarios (e.g., using cloud life cycles) still need to be investigated. The proposed algorithms need to be comprehensively evaluated (e.g., in cold seasons). Efforts are underway by the authors to improve the algorithm by testing more scenarios and we will report our findings in future.

Acknowledgements

Appendix A

A.1. Storm identification/segmentation

Similar to PERSIANN-CCS, the PERCAST model uses a segmentation algorithm named watershed transform (Roerdink and Meijster, 2001; Lakshmanan et al., 2009; Hong et al., 2004). This cloud-segmentation algorithm has a few definitions, as follows:

Seed: A seed is a cloud pixel with the relatively coldest pixel of each cold core. A cloud patch starts growing from a cold seed until reaching the terminated condition that can be a size or brightness temperature threshold.

Connectivity: The growing direction that was started from seed points for a 2-D.

Topography of cloud imagery: Assuming that the IR brightness temperature is well correlated with the height of the cloud according to the physical law of lapse rate, the lower temperature is associated with higher clouds in the troposphere. In a 3-D overview, the minimum BT represents the cloud-top overshooting points:

$$\tau(z) = -\frac{dT}{dz} \tag{A.1}$$

where the actual lapse rate $\tau(z)$ in the atmosphere will be a function of latent heat given to the air by condensation of water vapor. The lapse rate usually ranges in 6–10 K km^{-1}. T and z are temperature and altitude, respectively.

Segments: Conventionally, a segment is defined as a collection of adjacent pixels having similar values or gradual changes in values. The gradual change of BT is defined as Temperature Interval (TI).

Temperature Interval (TI): It is important how to gradually grow regions from seed points. The TI is a temperature interval to monitor the process of patch constitution. TI is estimated from the relationship between cloud BT and cloud height. Larger TI decreases the computation time and increases the undersegmentation of

cloud regions, as opposed to smaller TI, which increases the processing cost and may oversegment (Hong et al., 2004). PERCAST applies the TI equal to 10.

Topographical Hierarchical Thresholds (THT): Assuming the temperature minima as $T_{\min}$ and the discrimination threshold from clear sky as $T_{\max}$, THT is defined as:

$$THT = T_{\min} + TI \cdot i; \quad i = 1, 2, \ldots, m; \quad \text{where} \quad m$$
$$= \|(T_{\max} - T_{\min})/TI\| \tag{A.2}$$

The THT performs topographically top-down hierarchical thresholding from the cloud-top coldest core to the discrimination threshold (e.g., 235 K) (Griffith et al., 1978; Xu et al., 1999).

The algorithm primarily locates the coldest seeds $T_{\min}$ and then starts to iteratively expand each seed's area neighborhood size one at a time by including the border/warmer pixels until touching the separation threshold or the boundary of neighborhood patches. THT conducts a direct growing scheme in which colder pixels/regions join first.

Stepwise Seeded Region Growing (SSRG): The seed regions located on the coldest cores of cloud BT will grow up to the warmer region until touching the BT equal to THT = $T_{\min}$ + TI. Assuming that the process completes in m steps, then all related pixels colder than the specified THT$_m$ threshold are labeled as cloud regions. The process repeats the previous step until THT$_m \geqslant T_{\max}$.

Fig. A1 shows the application of the proposed algorithm to segment cloud imageries.

Appendix B

Appendix B describes the storm tracking algorithm.

B.1. Object-based storm tracking and matching

After storm identification/clustering, a tracking algorithm is applied to the identified cells. The object-based tracking algorithm matches the cells/objects from an image to the next one, corresponding to the same storm/cloud. As mentioned earlier, the PERCAST algorithm uses the pixel-based algorithm to track cloud pixels. PERCAST applies the contribution function to associate each storm object at time $t - 1$ to the corresponding storms at time t. The contribution function works based on the number of pixels that have been tracked using the pixel-based tracking algorithm. Using a technique that sets all contribution functions in a matrix helps to deal with complicated situations in which hundreds of storms occur simultaneously.

Figs. A2 and A3 present this technique. Fig. A2 shows the corresponding contribution matrix of the storm objects at time steps $t - 1$ and t, and Fig. A3 illustrates the storm objects from time steps $t - 1$ to t.

Assuming that n_1 and n_2 are the number of identified objects at time step $t - 1$ and t, rows are objects at time t and columns are objects at time $t - 1$. There are six rows ($n_2 = 6$) and five columns ($n_1 = 5$) (Fig. A2). The hypothetical numbers inside the matrix represent the contribution function between each two objects at time $t - 1$ and t.

The contribution matrix defines the relationship between objects at t and $t - 1$. For example, the $F_{A',A} = 0.4$ introduces the contribution of the object A' (time t) from object A (time $t - 1$) at about 0.4 or 40%. This algorithm calculates the contributed area of A' that actually comes from A using the pixel-based tracking algorithm. Considering a threshold ∼25% for acceptable contribution function of two storms (between $t - 1$ and t), the 40% contribution is large enough to associate two storms A and A'. Fig. A3 shows the final results in which two storm objects A and A' are associated. The $F_{F,A} = 0.1$ (Fig. A2) means that object A does not have a major

contribution in the generation of object F'. The contribution less than the threshold is not acceptable; hence, object F' is not associated to object A. Because object F' is not associated with any object at time $t - 1$ ($F_{F,B} = 0$, $F_{F,C} = 0$, $F_{F,D} = 0$, $F_{F,E} = 0$), it is a newly generated storm (Figs. A2 and A3). This matching process eventually associates all storm objects from $t - 1$ to t. If an object at time $t - 1$ (e.g., B) is connected with more than one object at time $t - 1$, it may be a split. Conversely, if one object at time t (e.g., C') is connected to more than one object at time $t - 1$, it may be a merger.

Separation threshold (t_{sep}): The parameter t_{sep} is an important parameter for the tracking-algorithm performance. As mentioned before, the proposed storm-tracking algorithm is defined based on the contribution function of storm objects between $t - 1$ and t. The contribution function shows what portion (or percentage) of each storm at time t is associated with any of the storms at time $t - 1$. The separation threshold (t_{sep}) is the minimum acceptable contribution function between two objects. As shown by Morel and Senesi (2002), smaller settings of t_{sep} can lead to some uncertainties for events in which storms are moving very close to each other.

Examining the sensitivity of t_{sep} with respect to different cloud BT and storm size can also be found from prior studies (Vila et al., 2008; Morel and Senesi, 2002). For approximately 75% of the large-scale storms, including MCS and tropical storms, the overlapping ratio is more than 60%. These studies have recommended a separation threshold t_{sep} of about 15–20% for larger-scale atmospheric events (e.g., MCS). For the purpose of this research, a conservative value of $t_{sep} = 0.25$ is selected to consider both large- and small-scale events.

Appendix C

It describes the storm feature extraction algorithm.

C.1. Storm-feature extraction

After completion of the cloud segmentation and tracking, cloud features should be extracted. The PERCAST-GD model projects each storm based on extracted features. This feature will be applied to estimate how the cloud evolves in the future. The following features will be used:

(1) Minimum temperature of each cloud object (BT_{min}).
(2) The minimum-temperature gradient for each storm object using time steps t, $t - 1$, and $t - 2$.

Considering there are two gradients, Grad ($BTmin_1$) and Grad ($BTmin_2$), determine how the cloud- minimum BT changes from time step $t - 1$ to $t - 2$ and t to $t - 1$, respectively, and the algorithm applies the average of two gradients as ΔBT_{min}:

$$\Delta BT_{min} = \frac{1}{2}\{Grad(BTmin_1) + Grad(BTmin_2)\} \qquad (C.1)$$

(3) Mean temperature of each cloud object (BT_{mean}).
(4) The mean-temperature gradient for each storm object using time steps t, $t - 1$, and $t - 2$. Considering there are two gradients Grad ($BTmean_1$) and Grad ($BTmean_2$), determine how the cloud-mean BT changes from time step $t - 1$ to $t - 2$ and t to $t - 1$, respectively, and the algorithm applies the average of two gradients as ΔBT_{mean}:

$$\Delta BT_{mean} = \frac{1}{2}\{(GradBTmean_1) + Grad(BTmean_2)\} \qquad (C.2)$$

(5) Each storm area (A).

(6) Growth and Decay (GD) trend: The PERCAST-GD algorithm uses each storm-size trend to extract GD coefficients. Three consecutive time steps, including $t - 2$, $t - 1$, and t, have been applied. ΔA_1 and ΔA_2 are the gradients of each storm object area from time $t - 2$ to $t - 1$ and $t - 1$ to t, respectively. The algorithm eventually applies ΔA, which is the average of the storm-object growth and decay trend. ΔA_1 and ΔA_2 greater than zero means object growth and vice versa.

$$Growth-Decay\ factor = \Delta A = \frac{1}{2}\{\Delta A_1 + \Delta A_1\} \qquad (C.3)$$

The PERCAST-GD projection module applies ΔA, ΔT_{min}, and ΔT_{mean} to project each storm object.

References

Adler, R.F., Huffman, G.J., Keehn, P.R., 1994. Global rain estimates from microwave-adjusted geosynchronous IR data. Remote Sens. Rev. 11, 125–152.

Afshar, A., Zahraei, A., Mariño, M., 2010. Large-scale nonlinear conjunctive use optimization problem: decomposition algorithm. J. Water Resour. Plann. Manage. 136 (1), 59–71. http://dx.doi.org/10.1061/(ASCE)0733-9496(2010)136:1(59).

Ashley, W., Mote, L., Dixon, P.G., Trotter, S.L., Powell, E.J., Durkee, J.D., Grundstein, A.J., 2003. Distribution of mesoscale convective complex rainfall in the United States. Mon. Weather Rev. 131 (12), 3003–3017.

Behrangi, A., Hsu, K., Imam, B., Sorooshian, S., Huffman, G.J., Kuligowski, R.J., 2009. PERSIANN-MSA: a precipitation estimation method from satellite-based multispectral analysis. J. Hydrometeorol. 10, 1414–1429.

Bellerby, T.J., 2006. High-resolution 2-D cloud-top advection from geostationary satellite imagery. IEEE Trans. Geosci. Remote Sens. 44 (12), 3639–3648.

Benjamin, S.G., Smirnova, T.G., Weygandt, S.S., Hu, M., Sahm, S.R., Jamison, B.D., Wolfson, M.M., Pinto, J.O., 2009. The HRRR 3-km storm resolving, radar-initialized, hourly updated forecasts for air traffic management. In: AMS Aviation, Range and Aerospace Meteorology Special Symposium on Weather-Air Traffic Management Integration, Phoenix, AZ.

Benjamin, S.G., Devenyi, D., Weygandt, S.S., Brundage, K.J., Brown, J.M., Grell, G.A., Kim, D., Schwartz, B.E., Smirnova, T.G., Smith, T.L., Manikin, G.S., 2004. An hourly assimilation-forecast cycle: the RUC. Mon. Weather Rev. 132, 495–518.

Berenguer, M., Sempere-Torres, D., Pegram, G.G.S., 2011. SBMcast – an ensemble nowcasting technique to assess the uncertainty in rainfall forecasts by Lagrangian extraplation. J. Hydrol. 404 (3–4), 226–240.

Chiang, Y.M., Chang, F.J., Jou, B., Lin, P.F., 2006. Dynamic ANN for precipitation estimation and forecasting from radar observations. J. Hydrol. 334 (1–2), 250–261.

Dixon, M., Wiener, G., 1993. TITAN: thunderstorm identification, tracking, analysis and nowcasting – a radar-based methodology. J. Atmos. Oceanic Technol. 10, 785–797.

Ganguly, A.R., Bras, R.L., 2003. Distributed quantitative precipitation forecasting using information from radar and numerical weather prediction models. J. Hydrometeorol. 4 (6), 1168–1180.

Germann, U., Zawadzki, I., 2002. Scale-dependence of the predictability of precipitation from continental radar images. Part I: description of the methodology. Mon. Weather Rev. 130 (12), 2859–2873.

Germann, U., Zawadzki, I., 2004. Scale-dependence of the predictability of precipitation from continental radar images. Part II: probability forecasts. J. Appl. Meteorol. 43 (1), 74–89.

Germann, U., Zawadzki, I., Turner, B., 2006. Predictability of precipitation from continental radar images. Part IV: limits to prediction. J. Atmos. Sci. 63, 2092–2108.

Golding, B.W., 1998. Nimrod: a system for generating automated very short-range forecasts. Meteorol. Appl. 5 (1), 1–16.

Grecu, M., Krajewski, W.F., 2000. A large-sample investigation of statistical procedures for radar-based short-term quantitative precipitation forecasting. J. Hydrol. 239 (1–4), 69–84.

Griffith, C.G., Woodley, W.L., Grube, P.G., Martin, D.W., Stout, J., Sikdar, D.N., 1978. Rain estimation from geosynchronous satellite imagery – visible and infrared studies. Mon. Weather Rev. 106, 1153–1171.

Hogan, R., O'Connor, E., Illingworth, A., 2009. Verification of cloud-fraction forecasts. Quart. J. Roy. Meteor. Soc. 135, 1494–1511.

Hong, Y., Hsu, K., Sorooshian, S., Gao, X., 2004. Precipitation estimation from remotely sensed imagery using an artificial neural network cloud classification system. J. Appl. Meteorol. 43 (12), 1834–1853.

Hong, Y., Hsu, K., Sorooshian, S., Gao, X., 2005. Self-organizing nonlinear output (SONO): a neural network suitable for cloud patch-based rainfall estimation at small scales. Water Resour. Res. 41, W03008. http://dx.doi.org/10.1029/2004WR003142.

Hsu, K.L., Gupta, H.V., Gao, X., Sorooshian, S., 1999. Estimation of physical variables from multichannel remotely sensed imagery using a neural network: application to rainfall estimation. Water Resour. Res. 35, 1605–1618.

Janowiak, J.E., Joyce, R.J., Yarosh, Y., 2001. A real-time global half-hourly pixel-resolution infrared dataset and its applications. Bull. Am. Meteorol. Soc. 82 (2), 205–217.

Johnson, J.T., MacKeen, P.L., Witt, A., Mitchell, E.D., Stumpf, G.J., Eilts, M.D., Thomas, K.W., 1998. The storm cell identification and tracking algorithm: an enhanced WSR-88D algorithm. Weather Forecast. 13 (2), 263–276.

Lakshmanan, V., Fritz, A., Smith, T., Hondl, K., Stumpf, G.J., 2007. An automated technique to quality control radar reflectivity data. J. Appl. Meteorol. Climatol. 46, 288–305.

Lakshmanan, V., Hondl, K., Rabin, R., 2009. An efficient, general-purpose technique for identifying storm cells in geospatial images. J. Atmos. Oceanic Technol. 26, 523–537.

Legates, D.R., McCabe Jr., G.J., 1999. Evaluating the use of "goodness-of-fit" measures in hydrologic and hydroclimatic model validation. Water Resour. Res. 35 (1), 233–241.

Liang, Q., Feng, Y., Deng, W., Hu, S., Huang, Y., Zeng, Q., Chen, Z., 2010. A composite approach of radar echo extrapolation based on TREC vectors in combination with model-predicted winds. Adv. Atmos. Sci. 27 (5), 1119–1130. http://dx.doi.org/10.1007/s00376-009-9093-4.

Machado, L.A.T., Rosso, W.B., Guedes, R.L., Walker, A.W., 1998. Life cycle variations of mesoscale convective systems over the Americas. Mon. Weather Rev. 126 (6), 1630–1654.

Machado, L.A.T., Laurent, H., 2004. The convective system area expansion over Amazonia and its relationships with convective system life duration and high-level wind divergence. Mon. Weather Rev. 132 (3), 714–725.

Mecklenburg, S., Joss, J., Schmid, W., 2000. Improving the nowcasting of precipitation in an Alpine region with an enhanced radar echo tracking algorithm. J. Hydrol. 239 (1–4), 46–68.

Montanari, L., Montanari, A., Toth, E., 2006. A comparison and uncertainty assessment of system analysis techniques for short-term quantitative precipitation nowcasting based on radar images. J. Geophys. Res. 111, D14111. http://dx.doi.org/10.1029/2005JD006729, 12 p.

Mathon, V., Laurent, H., 2001. Life cycle of Sahelian mesoscale convective cloud systems. Quart. J. Roy. Meteor. Soc. 127 (572), 377–406.

Morel, C., Orain, F., Senesi, S., 1997. Automated detection and characterization of MCS using the meteosat infrared channel. In: Proceedings of the Meteorological Satellite Data Users Conference. Brussels, Belgium, EUMETSAT, pp. 213–220.

Morel, C., Senesi, S., 2002. A climatology of mesoscale convective systems over Europe using satellite infrared imagery. I: methodology. Quart. J. Roy. Meteor. Soc. 128 (584), 1953–1971.

Mueller, C., Saxen, T., Roberts, R., Wilson, J., Betancourt, T., Dettling, S., Oien, N., Yee, J., 2003. NCAR auto-nowcast system. Weather Forecast. 18 (4), 545–561.

Roerdink, J., Meijster, A., 2001. The watershed transform: definitions, algorithms and parallelization strategies. Fundam. Inform. 41 (3), 187–228.

Scofield, R., Kuligowski, R., Davenport, C., 2004. The use of the Hydro-Nowcaster for mesoscale convective systems and the Tropical Rainfall Nowcaster (TRaN) for landfalling tropical systems. In: Preprints, Symposium on Planning, Nowcasting, and Forecasting in the Urban Zone, Seattle, WA, American Meteorological Society, 1.4.

Sokol, Z., 2006. Nowcasting of 1-h precipitation using radar and NWP data. J. Hydrol. 328 (1–2), 200–211.

Sokol, Z., Pesice, P., 2012. Nowcasting of precipitation–advection statistical forecast model (SAM) for the Czech Republic. J. Atmos. Res. 103, 70–79.

Stephenson, D., 2000. Use of the "odds ratio" for diagnosing forecast skill. Weather Forecast. 15, 221–232.

Vant-Hull, B., Ba, M., Rabin, R., Mahani, D.S., Kuligowski, R.J., Gruber, A., Smith, S.B., 2008. Transitioning GOES-based nowcasting capability into the GOES-R era. In: Proceedings of the 5th GOES Users' Conference, New Orleans, LA, pp. 213–220.

Vasiloff, S.V., Seo, D.J., Howard, K.W., Zhang, J., Kitzmiller, D.H., Mullusky, M.G., Krajewski, W.F., Brandes, E.A., Rabin, R.M., Berkowitz, D.S., Brooks, H.E., McGinley, J.A., Kuligowski, R.J., Brown, B.G., 2007. Improving QPE and very short term QPF: an initiative for a community-wide integrated approach. Bull. Am. Meteorol. Soc. 88, 1899–1911.

Vila, D.A., Machado, L.A.T., Laurent, H., Velasco, I., 2008. Forecast and tracking the evolution of cloud clusters (ForTraCC) using satellite infrared imagery: methodology and validation. Weather Forecast. 23, 233–245.

Wilson, J.E., Ebert, E., Saxen, T.R., Roberts, R.D., Mueller, C.K., Sleigh, M., Pierce, C.E., Seed, A., 2004. Sydney 2000 forecast demonstration project: convective storm nowcasting. Weather Forecast. 19, 131–150.

Xu, L., Gao, X., Sorooshian, S., Arkin, P.A., Imam, B., 1999. A microwave infrared threshold technique to improve the GOES precipitation index. J. Appl. Meteorol. 38, 569–579.

Zahraei, A., Hsu, K., Sorooshian, S., 2010a. Severe storms nowcasting: using cloud advection field. American Geophysical Union Proceeding, vol. 1. American Geophysical Union, San Francisco, CA, U.S.A, pp. 1141–1146, <http://adsabs.harvard.edu/abs/2010AGUFM.H33B1141H>.

Zahraei, A., Gourley, J.J., Hong, Y., Lakshmanan, V., Hsu, K., Sorooshian, S., 2010b. Pixel-based very short-term precipitation forecasting for hydrological application. American Geophysical Union Proceeding, vol. 1. American Geophysical Union, San Francisco, CA, U.S.A, pp. 1111–1116, <http://adsabs.harvard.edu/abs/2010AGUFM.H21E1111Z>.

Zahraei, A., Hsu, K., Sorooshian, S., Behrangi, A., 2011a. Advection-based short-term quantitative precipitation forecasting algorithm using radar and satellite information. American Geophysical Union Proceeding, vol. 1. American Geophysical Union, San Francisco, CA, U.S.A, pp. 2–6, <http://adsabs.harvard.edu/abs/2011AGUFM.H13I..02Z>.

Zahraei, A., Hsu, K., Sorooshian, S., Behrangi, A., 2011b. Short-term severe storm forecasting using an object-based tracking technique. American Meteorological Conference Proceeding, 18th Conference on Satellite Meteorology, Oceanography and Climatology, vol. 1. American Meteorological Society, New Orleans, LA, U.S.A, pp. 1–8, <https://ams.confex.com/ams/92Annual/webprogram/Paper201880.html>.

Zahraei, A., Hsu, K., Sorooshian, S., Gourley, J.J., Hong, Y., Lakshmanan, V., Bellerby, T., 2012. Short-term quantitative precipitation forecasting: a Lagrangian pixel-based approach. J. Atmos. Res., 418–434, <http://www.sciencedirect.com/science/article/pii/S0169809512002219>.

Zhang, J. et al., 2011. National mosaic and multi-sensor QPE (NMQ) system: description, results, and future plans. Bull. Am. Meteorol. Soc. 92, 1321–1338.